LIDS-P-2244
April 1994

Estimation of Dynamically Evolving Ellipsoids with Applications to Medical Imaging [1]

Seema Jaggi William C. Karl

Alan S. Willsky

Laboratory for Information and Decision Systems

Department of Electrical Engineering and Computer Science

Massachusetts Institute of Technology

Cambridge, Massachusetts, 02139

Telephone: (617) 253-3816

Telefax: (617) 258-8553

Email: jaggi@athena.mit.edu

[1]This research was conducted with support provided in part by the National Science Foundation under grant 9015281-MIP, Army Research Office under grant DAAL03-92-G-0115 and the Office of Naval Research under grant N00014-91-J-1004.

Abstract

This research deals with the estimation of dynamically evolving ellipsoids from noisy observations (e.g. lower-dimensional projections). By appropriately choosing the representations for ellipsoids, their dynamics, and their projections, it is possible to reconstruct such a dynamically evolving ellipsoid using the well-developed results and methods of recursive estimation theory. Specifically, this work concentrates on a medical imaging application of ellipsoid estimation where the precise ellipsoid dynamics and projection geometries are unknown.

The medical application considered in this paper is a method to obtain a dynamic estimate of left-ventricular ejection fraction from a gated set of planar myocardial perfusion images from three views. Ejection fraction, defined as the ratio of the fully contracted left-ventricular volume to the fully expanded left-ventricular volume, is known as an effective gauge of cardiac function. Thus, myocardial perfusion images may be used to estimate ejection fraction as well as to locate infarcts. This may lead to a more cost-effective diagnostic procedure which limits the patient's exposure to radiation.

To formulate this estimate of ejection fraction, geometric reconstruction and recursive estimation techniques are employed. The left ventricle is modeled as a dynamically evolving three-dimensional ellipsoid. The left-ventricular outline observed in the myocardial perfusion images is then modeled as a dynamic, two-dimensional ellipse, obtained as the projection of the former three-dimensional ellipsoid. This data is processed in two ways. In the first, the three views are processed together as a three-dimensional dynamic ellipsoid reconstruction problem. An alternative method is to process each view individually as a two-dimensional dynamic ellipse estimation problem and calculate a three-dimensional ejection fraction based on the effective two-dimensional ejection fractions of each view. Both methods are investigated.

The approximating ellipsoids are reconstructed using a Rauch-Tung-Striebel smoothing filter which combines the observed temporal set of projection images with an evolution model to produce the best estimate of the ellipsoid at any point in time given all the data. This method produces an ejection fraction estimate which is more robust to noise. Further, numerical studies of the sensitivity of this approach to unknown dynamics and projection geometry are presented, providing a rational basis for specifying system parameters and data requirements. This investigation includes estimation of ejection fraction from both simulated and real data.

Keywords: ellipsoids, geometric reconstruction, ejection fraction, myocardial perfusion

1 INTRODUCTION

This research deals with an application in medical imaging of estimation of dynamically evolving ellipsoids from noisy observations (often obtained as lower-dimensional projections). Much work in geometric reconstruction [1–5] has focused on reconstructing objects such as ellipsoids from noisy lower-dimensional projections. While past work in this area has focused on static objects or dynamically evolving objects with known dynamics and projection geometry, the work presented in this paper deals with the reconstruction of a dynamically evolving ellipsoid from noisy observations when the dynamics of the object and the observation geometry may be imprecisely known. This is the case in many practical applications such as medical imaging.

In particular, this work concentrates on a method to obtain the ejection fraction of the left ventricle of the heart from a gated set of planar radionuclide (^{99m}Tc) myocardial perfusion images [6–8]. The ejection fraction of the left ventricle has long been known as an effective gauge of cardiac function [9]. Gated myocardial perfusion imaging is a radionuclide technique that may be used to produce a sequential set of images of the heart in motion. The model-based approach described in this paper employs geometric reconstruction and recursive estimation techniques to track left-ventricular shape throughout the cardiac cycle, thus allowing the generation of a *dynamically-based* ejection fraction estimate.

The ejection fraction (EF) is a measure of the pumping capability of the heart and has great prognostic value to cardiologists. The ejection fraction is defined as:

$$\mathrm{EF} = 1 - \frac{\text{end systolic volume}}{\text{end diastolic volume}} \tag{1}$$

where end systole and end diastole are the fully contracted and fully expanded cardiac phases, respectively. A reduced ejection fraction is indicative of impaired cardiac function.

In this work, the ejection fraction estimate is based on data obtained from a temporal set of

myocardial perfusion images [6–8] from three views which are obtained by injecting the patient with a radionuclide marked substance (^{99m}Tc in this case) and imaging with a gamma camera. The gamma camera produces images by counting the photons emitted from the radioactive tracer. Since small doses must be used for safety reasons, the images are produced via ECG-gating. The resulting ECG-gated myocardial perfusion images are not snapshots of the heart in motion, but rather, the sum of a particular cardiac phase over many cardiac cycles. The data-acquisition modality coupled with beat-to-beat variability, combine to give poor visual quality images. The resulting temporal set of images are taken at 16 equally spaced points in the cardiac cycle. Typically, the data set consists of images from three views: anterior (ANT), lateral (LAT), and left anterior oblique (LAO). Anterior is a frontal view; lateral is a side view underneath the left arm; and left anterior oblique is a frontal view skewed down and to the left side. Figure 1 shows a sample myocardial perfusion image from the ANT view.

A gated set of myocardial perfusion images are used here to estimate ejection fraction, a purpose for which they are not traditionally used. Myocardial perfusion images, while of poor visual quality, contain a large amount of *physiological* information reflecting the tie between the chosen radionuclide and the biochemistry of the region under study. As a result, these images are traditionally used to locate infarcts, areas in the heart muscle that are being deprived of nutrients because of an occlusion in the vessels of the heart. In the myocardial perfusion images, such infarcts appear as dark regions due to the lack of radionuclide reaching the region. In addition to this traditional role, it is possible to distinguish the outline of the left-ventricular chamber from myocardial perfusion images and thus, also obtain *structural* information. It is this projection-like outline of the left-ventricular chamber that is used in this work to track left-ventricular volume and estimate ejection fraction.

Geometric reconstruction and recursive estimation techniques are used here to formulate

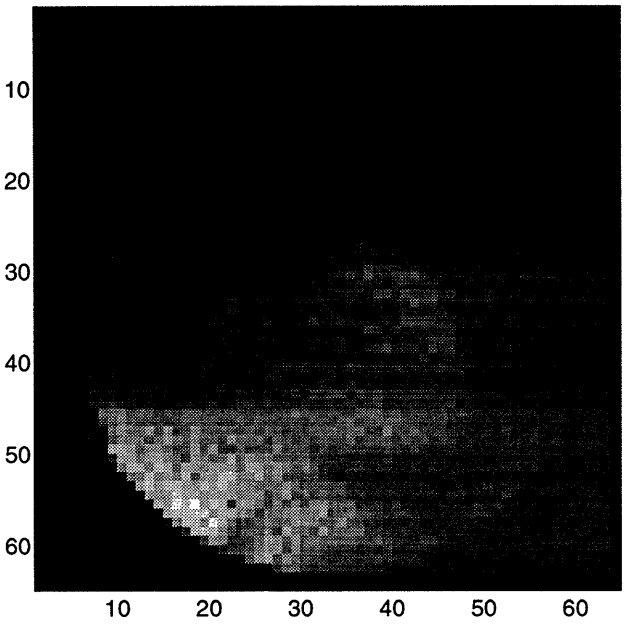

Figure 1: A sample myocardial perfusion image. The horseshoe shaped object in the center is the left-ventricular wall and the bright object in the lower left is the liver.

an ejection fraction estimate based on myocardial perfusion images. One commonly used approximation to the true shape of the left ventricle is a three-dimensional ellipsoid [10–12]. The projections (or shadows) of this left-ventricular ellipsoidal model are then two-dimensional ellipsoids, which model the left-ventricular outline in the observed myocardial perfusion images. In this work, by projections, we mean the shadow projection of this ellipsoidal shape, rather than line integral projections. As previously mentioned, much work in geometric reconstruction has focused on reconstructing objects such as ellipsoids from noisy lower-dimensional projections. Combining these geometric reconstruction techniques with statistical recursive estimation procedures, such as Rauch-Tung-Striebel smoothing[1] [13], it is possible to formulate an estimation procedure that combines the observed temporal set of projection images

[1]Rauch-Tung-Striebel smoothing is an efficient algorithm to find the optimal estimate at any point in time given all the data over an interval.

with an evolution model to produce the best estimate of the ellipsoid at any point given all the data. We examine two ways of processing the projection data. In the first, the three projection views are processed together as a single three-dimensional ellipsoid reconstruction problem. An alternative, simpler method, which still utilizes the data from all three views, is to process each view individually as a two-dimensional dynamic ellipse estimation problem and then to calculate a three-dimensional ejection fraction based on the effective two-dimensional ejection fractions obtained from each view. Both techniques are investigated in order to assess robustness to inevitable errors in the knowledge of the three image or projection planes.

Many techniques exist for estimating ejection fraction including angiography [10], echocardiography [14], magnetic resonance imaging [15], and radionuclide ventriculography [10,16]. The "gold standard" (GS) estimate of ejection fraction used here is based on multiple-gated blood pool (MUGA) images. The ultimate objective of this work will be to show a high degree of correlation between our ejection fraction estimates based on myocardial perfusion images and standard estimates based on MUGA. Several important points should be noted in comparing ejection fraction estimates based on myocardial perfusion images to those based on MUGA. First, an ejection fraction estimate based on myocardial perfusion images provides a safer and more cost-effective alternative to the MUGA based estimates. This is because the typical diagnostic procedure includes both the myocardial perfusion imaging to obtain physiological information about possible cardiac infarcts and the MUGA imaging to estimate ejection fraction. Thus, by estimating ejection fraction from myocardial perfusion images alone, the need for MUGA imaging could be eliminated and the patient's exposure to radiation minimized. Second, the smoothing techniques used in this work combine *all the frames* of data (in contrast to current techniques) to give an ejection fraction estimate, which is more robust to variations due to noise. Third, in a formulation based on geometric reconstruction and statistical meth-

ods, the modeling assumptions are explicitly stated. Thus, it is possible to investigate the sensitivity of the estimate with respect to these assumptions. Indeed, we do precisely that in Section 3.

In addition, note that the dynamically-based smoothing techniques presented in this work are also directly applicable to ejection fraction estimates from other types of data. Again, our dynamically-based smoothing techniques combine several frames of data to give an ejection fraction estimate which is more robust to variations due to noise than those methods using only single frames of data. For example, a similar smoothing filter-based reconstruction could be applied to MUGA images or even angiographic data, also yielding more accurate ejection fraction estimates from those modalities.

The organization of this paper is as follows. In Section 2, the necessary background from geometric reconstruction and statistical recursive estimation is discussed together with their application to the estimation of ejection fraction from myocardial perfusion images. Section 3 presents numerical experiments examining our methods and results as applied to simulated data. Finally, in Section 4, ejection fraction estimates from real myocardial perfusion images are presented.

2 PROBLEM FORMULATION

As previously mentioned, we model the left ventricle and its projections as dynamically evolving ellipsoids. Thus, the myocardial perfusion images are viewed as noisy two-dimensional projections of a dynamically evolving three-dimensional ellipsoid. Using the approach described in [3] it is possible to reconstruct an n-dimensional dynamic ellipsoid from noisy observations, e.g. lower-dimensional projections. This section summarizes the mathematical formulation in-

volving reconstruction of an n-dimensional dynamically evolving ellipsoid and discusses the issues arising in its application to the processing of myocardial perfusion images to estimate ejection fraction.

2.1 Mathematical Background

Consider the general problem of reconstructing a dynamically evolving n-dimensional ellipsoid from a series of noisy (perhaps lower-dimensional projection) observations. This problem may be greatly simplified by choosing appropriate representations for the ellipsoids and their dynamics. Several such representations (including the one used in this work) are discussed in detail in [3]. It is possible to represent the points included in an n-dimensional, origin centered, non-degenerate ellipsoid in the following way:

$$\{z | z^T X^{-1} z \leq 1, z \in R^n\} \tag{2}$$

where the symmetric, positive definite, $n \times n$ matrix X that represents the ellipsoid is easily determined. For example, a two-dimensional ellipsoid (an ellipse) centered at the origin with semi-axis lengths, a and b, and an angle of rotation ϕ is represented by the matrix:

$$X = \begin{pmatrix} \cos\phi & \sin\phi \\ -\sin\phi & \cos\phi \end{pmatrix}^T \begin{pmatrix} a^2 & 0 \\ 0 & b^2 \end{pmatrix} \begin{pmatrix} \cos\phi & \sin\phi \\ -\sin\phi & \cos\phi \end{pmatrix}$$

The projections of an ellipsoid are themselves ellipsoids of lower dimension. The symmetric matrix representation of the ellipsoid (2) yields a linear relationship between the matrix X that represents the ellipsoid and the matrix Y_i that represents the ellipsoid in a given projection. In particular, this relationship is given by:

$$Y_i = C_i^T X C_i \tag{3}$$

where the matrix C_i captures the geometry of the projection. Specifically, the rows of the matrix C_i span the space of the projection. Note that the case where C_i is the identity corresponds to observations of the ellipsoid itself.

Representing an ellipsoid by its associated matrix X, it is possible to capture a broad range of ellipsoid dynamics through the following evolution equation:

$$X(k+1) = A(k)^T X(k) A(k) \tag{4}$$

where changes such as magnification, rotation, and eccentricity change may be included in a simple way in $A(k)$. For example, in the two-dimensional case, one convenient choice for the matrix that captures the dynamics is given by (see [5]):

$$A(k) = \begin{pmatrix} c(k) & 0 \\ 0 & c(k) \end{pmatrix} \begin{pmatrix} \alpha(k) & 0 \\ 0 & 1/\alpha(k) \end{pmatrix} \begin{pmatrix} \cos\theta(k) & \sin\theta(k) \\ -\sin\theta(k) & \cos\theta(k) \end{pmatrix} \tag{5}$$

where the first term represents uniform scaling by the factor $c(k) \geq 0$, the second term represents an area preserving stretching along the coordinate axes by $\alpha(k) \geq 0$, and the last term represents rotation by an angle $\theta(k)$. This general form is easily extended to express similar dynamics for ellipsoids of higher dimensions.

Now if we have *noisy* observations of the evolving matrix $X(k)$ of the form (3), these may be captured by the observation equation:

$$Y_i(k) = C_i^T X(k) C_i + V_i(k) \tag{6}$$

where the symmetric matrix $V_i(k)$ represents the effects of observation noise. Note that this model assumes that our observations are actually ***ellipsoids***, with the uncertainty appearing in the exact shape of the ellipsoid. To simplify the ellipsoid reconstruction problem, we assume

that the independent elements of $V_i(k)$ have a Gaussian distribution[2].

By casting the geometrically intuitive formulas (4) and (6) in standard state space form, it is possible to invoke the well-developed methods of recursive estimation theory and still preserve the geometric interpretation of the original problem formulation. To this end, note that the set of $n \times n$ symmetric matrices forms a $\frac{n(n+1)}{2}$-dimensional vector space. Thus, there exists an *equivalent* vector representation for the linear ellipsoid dynamics (4) and observation equation (6) given by:

$$x(k+1) = \tilde{A}(k)\, x(k) \tag{7}$$

$$y(k) = \tilde{C}\, x(k) + v(k) \tag{8}$$

where the matrices $\tilde{A}$ and $\tilde{C}$ are matrix representations of the linear operators on $X(k)$ defined in (4) and (6) with respect to given orthonormal bases on the sets of symmetric matrices of corresponding dimension. Thus, there is a one-to-one correspondence between $X(k)$ and $x(k)$ (similarly between $Y(k)$ and $y(k)$) and our intuition about the ellipsoid evolution and measurement equations is preserved. In [3], specific orthonormal bases and thus forms for the matrices $\tilde{A}$ and $\tilde{C}$ are discussed. More exactly, the matrix $\tilde{C}$ is obtained by stacking the matrix representations of each of the linear operators C_i. Further, it follows from (6) that the term $v(k)$ is a Gaussian vector with zero mean and variance $R = rI$. The important feature of the formulation in (7) and (8) is that the problem is now stated in the standard state space framework (i.e. tracking a dynamically evolving state vector from noisy measurements), which is directly amenable to the extensive set of techniques from recursive estimation. In particular,

[2]This model is not strictly proper, since it implies that $Y_i(k)$ will not always be a positive definite matrix, which it must be to represent an ellipsoid. However, we choose to employ this commonly-used assumption because of the simplification it provides in the ellipsoid reconstruction problem. Other more complicated models are, of course, possible.

the Rauch-Tung-Striebel (RTS) smoothing algorithm [13] may be used to obtain $\hat{x}(k|T)$, the best estimate of the ellipsoid $x(k)$ at time k given data over the entire time interval $[0, T]$.

2.2 Application to Processing of Myocardial Images

The RTS smoothing algorithm will be used throughout this work to reconstruct ellipsoids that approximate both the left ventricle and its projections. The left-ventricular ejection fraction will then be calculated from the temporal volume changes of these reconstructed ellipsoids using (1). Recall that the formulation of (6) assumes that it is ellipsoids (albeit perturbed ones) and not images that are our observations. Thus, in our work with myocardial image data a preprocessing step which extracts ellipses from the raw images will be assumed. There exist many such methods to extract ellipses from planar data [17–19]. In a practical setting, the statistics of $v(k)$ in (8) would be provided by this preprocessing step. Since this is not the focus of this paper, we assume that such a preprocessing step which extracts ellipses and provides the statistics of the measurement noise is available.

Before proceeding, note that the transformation from the ellipsoid shape, as specified by the symmetric matrix $X(k)$ (or equivalently by $x(k)$), to the ejection fraction is a nonlinear one. In particular, the volume of the ellipsoid is proportional to the square root of the determinant of $X(k)$. This nonlinearity is then combined with the further nonlinearity in the definition (1) to obtain the ejection fraction. In addition, note that this transformation between ellipses and ejection fraction is not one-to-one since many combinations of different maximum and minimum ellipses will yield the same ejection fraction.

There are a number of ways that we can imagine using the formulation in Section 2.1 to combine the information in the different projection views. We will only consider the following two here, though others can be imagined. The first, and perhaps most straightforward, ap-

proach is to process the three projection views together in a single three-dimensional ellipsoid reconstruction problem, i.e. our observations are taken to be two-dimensional projections of an underlying three-dimensional ellipsoid. An ejection fraction estimate is then based on the resulting reconstructed three-dimensional dynamic ellipsoid according to (1). Of course, this type of processing inherently requires that a projection geometry be specified.

An alternative, simpler method, which we also consider, is to process each lower-dimensional view individually as an independent two-dimensional ellipse estimation problem, thus obtaining three, two-dimensional dynamic ellipse estimates. In this case, our observations are taken as the two-dimensional ellipses themselves. For each of these three dynamic ellipse estimates, a corresponding apparent planar "ejection fraction" can be found. The overall ejection fraction may then be obtained by combining these two-dimensional ejection fractions calculated from each view under certain simplifying assumptions. In particular, this combination may be accomplished using the following easily derived formula relating the ejection fraction of a 3-D ellipsoid to the apparent ejection fractions of its projections onto mutually orthogonal planes aligned with the ellipsoid axes:

$$\mathrm{EF} = 1 - \sqrt{(1 - \mathrm{EF}_{\mathrm{view1}})(1 - \mathrm{EF}_{\mathrm{view2}})(1 - \mathrm{EF}_{\mathrm{view3}})} \tag{9}$$

where EF is the overall ejection fraction of the 3D ellipsoid and $\mathrm{EF}_{\mathrm{view}i}$ is the apparent ejection fraction of the ellipses in projection i. Note that this formulation also inherently assumes a projection geometry, i.e. projections onto orthogonal planes aligned with the semi-axes of the ellipsoid.

Regardless of which way we choose to use the results of Section 2.1 to combine the data, there are two significant obstacles to be addressed to obtain reliable dynamic shape reconstructions and ejection fraction estimates from the real data. First, the underlying ellipsoid

dynamics, as captured by $A(k)$, are unknown to us (though we clearly have significant prior knowledge in this regard). Second, the projection geometry, as captured explicitly in C or implicitly in equation (9), is variable and, further, imperfectly known. Past work in geometric reconstruction [3] concentrated on reconstruction of dynamically evolving ellipsoids from lower-dimensional projections with known dynamics and projection geometries. Next we discuss methods to overcome our lack of knowledge about the dynamics and projection geometry. These methods are combined to yield our overall approach. The methods proposed in this section and their sensitivity are examined through numerical simulations in Section 3.

Imperfectly Known Dynamics

The dynamics of the ellipsoid which approximates the left ventricle are unknown. The true left-ventricular dynamics vary from person to person and from cycle to cycle. Thus, some way of identifying or approximating these dynamics is needed. The approach used in this work employs a model identification scheme based on hypothesis testing to determine a coarse approximation to the true ellipsoid dynamics. The RTS smoothing filter reconstruction is then based on the dynamics chosen by the model identification scheme. Note that because the model identification yields only a coarse approximation to the true dynamics, model mismatch will still remain in the smoothing filter reconstruction, and we discuss how to account for this effect later in this section.

Hypothesis testing is used to perform the coarse model identification by determining which of several hypothesized models best accounts for the observed ellipsoid behavior given all of the measurements. Such a scheme is particularly amenable for estimating the dynamics of the ellipsoid that approximates the left ventricle because we may use our prior knowledge of heart behavior to define a small set of reasonable hypotheses. In particular, although

the precise dynamics of the left ventricle are unknown, it is reasonable to assume that the underlying left-ventricular dynamics correspond to a uniform shrinking phase followed by a uniform expansion phase, the only uncertainty being in the rate. Thus, each hypothesized model may be formulated to incorporate this prior knowledge of left-ventricular behavior with an associated hypothesized rate parameter and associated ejection fraction. Since it is ejection fraction that is of interest to us and each model has associated with it a corresponding (unique) ejection fraction, in what follows we will often refer to these different models by these associated ejection fractions with the understanding that it is actually the underlying dynamic model to which we refer.

Model identification is a stochastic estimation technique which determines which of several hypothesized models is most likely given the data. That is, the model identifier chooses model i from m hypothesized models at time k if model i maximizes the quantity:

$$\mathrm{p}_i(k) = \Pr(\text{model } i \text{ is correct} | \mathcal{Y}_k) \tag{10}$$

where $\mathcal{Y}_k$ is the set of measurements up to and including the measurement at time k. Applying Bayes' rule, (10) is rewritten in the following recursive form:

$$\mathrm{p}_i(k) = \frac{\mathrm{p}(y(k)|\mathcal{Y}_{k-1}, \text{model } i \text{ is correct})\, \mathrm{p}_i(k-1)}{\sum_{j=1}^{m} \mathrm{p}(y(k)|\mathcal{Y}_{k-1}, \text{model } j \text{ is correct})\, \mathrm{p}_j(k-1)} \tag{11}$$

The quantity $\mathrm{p}(y(k)|\mathcal{Y}_{k-1}, \text{model } i \text{ is correct})$ is obtained as a byproduct of the Kalman filter based on model i and is given by

$$\mathrm{p}(y(k)|\mathcal{Y}_{k-1}, \text{model } i \text{ is correct}) = \mathrm{N}(\nu_i(k); 0, \mathcal{V}_i(k)) \tag{12}$$

where $\nu_i(k)$ are the Kalman filter residuals at time k under hypothesis i and $\mathrm{N}(\nu_i(k); 0, \mathcal{V}_i(k))$ is a a Gaussian distribution with mean of zero and variance $\mathcal{V}_i(k)$ evaluated at $\nu_i(k)$. Both $\nu_i(k)$ and $\mathcal{V}_i(k)$ are obtained directly from the Kalman filter. By substituting (12) in (11), it is

possible to calculate $p_i(k)$. Thus, the model identification scheme consists of a bank of Kalman filters, one based on each of the hypothesized models, and a comparison step to determine which hypothesized model maximizes $p_i(T)$, where T is the time interval over which we have data. In Section 3.1 we present some numerical experiments demonstrating the performance of such an approach.

At best, the model identification phase yields only a coarse approximation to the underlying cardiac dynamics. Thus, the smoothing filter, which is based on the output of the model identifier, will produce ellipsoid, and hence ejection fraction, estimates which are undoubtedly corrupted by this residual dynamic model mismatch. In particular, suppose the smoothing filter equations are implemented based on the dynamic matrices $A(k)$, which are an approximation to the true (unknown) dynamics of the system. One approach to compensating for this error introduced by dynamic model mismatch is through the addition of a process noise term to the modeled dynamics in (7) on which we will base our filter; that is, the error introduced by dynamic model mismatch is modeled as a process noise with a variance of $Q = qI$. In general, the smoothed state estimate at any time is a weighted average of the measured and predicted states. In the smoothing filter, the variance of such a process noise term may be interpreted as a measure of the trust in the dynamic model, and thus the predicted state versus the measured data. If q is very high, the estimate will be based on the measurements alone. If q is low, the estimate will be based on the predicted state (and thus the dynamic model and initial condition) alone. Hence, the value of q may be used to compensate for the effect of dynamic model mismatch by reducing the dependence on the model in the estimate.

Imperfectly Known Projection Geometry

Beyond imperfect knowledge of the ellipsoid dynamics, the relationship between the ellipsoid and our projection observations of it, i.e. the projection geometry, are imperfectly known. In particular, the positioning of the gamma camera used to produce the myocardial perfusion images is not exact or precisely measured. While the camera is positioned to obtain roughly the ANT, LAT and LAO views, the exact position varies from patient to patient. One can imagine developing a further hypothesis testing procedure to estimate the projection geometry. However for this work, we will simply assume orientations for the three projection planes then examine the sensitivity of our reconstructions to this assumption.

We expect that the effect of errors in this assumed projection geometry on the resulting *ejection fraction* estimate to be minimal for the following reasons. First, the left ventricle is a minimally eccentric ellipsoid; its shape tends towards a sphere. The projections of such a minimally eccentric ellipsoid are roughly equivalent on all planes. Thus, the assumed projection geometry introduces minimal error in the ejection fraction estimate. Second, the dynamics of the left ventricle include only a slight rotation. For the simple case where the dynamics consist of only isotropic contraction without rotation, it is easy to show that the assumed projection geometry does not introduce *any* error into the ejection fraction estimate. Even for more complicated dynamics, which include isotropic contraction and a gross rotation, the effect of the assumed projection geometry on the ejection fraction estimate is minimal. We demonstrate this through a sensitivity analysis in Section 3.

Three-Dimensional Processing

Let us begin by discussing our three-dimensional approach to processing of the data that was mentioned earlier in this section. In this method the three views are processed together as a

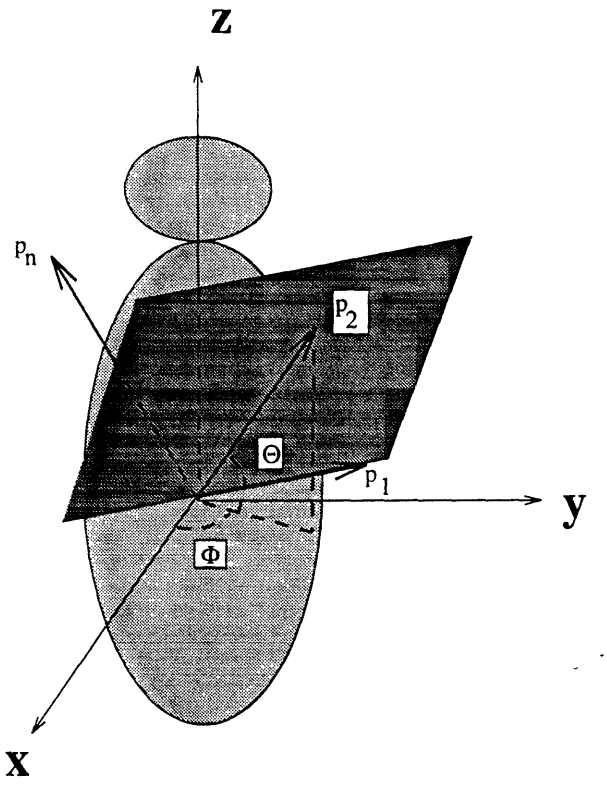

Figure 2: Projection plane orientation.

single three-dimensional model identification/reconstruction problem. That is, the model identifier and smoothing-filter-based reconstruction are used to reconstruct the three-dimensional ellipsoid that best approximates the left ventricle based on the set of noisy two-dimensional projections in the three views. The outcome of the model identifier is used to provide a dynamic model for the smoothing-filter-based reconstruction. Based on the volume of the estimated three-dimensional ellipsoids which are the output of the smoothing filter, an estimate of the ejection fraction is calculated according to (1). Since the true projection geometry is unknown, we use an assumed projection geometry that approximates the standard ANT, LAT, and LAO views. In particular, we assume our three projections are onto the xz-plane, the yz-plane, and a plane which is tilted at an angle $\Theta = 45°$ from the xy-plane about an axis, p_1 that forms an angle $\Phi = 45°$ with the y-axis, as shown in Figure 2. This third plane is completely specified

by its normal, p_n.

$$p_n = (-\cos\Phi\sin\Theta, -\sin\Phi\sin\Theta, \cos\Theta) \tag{13}$$

This assumed (or modeled) projection geometry are captured in (6) by the set of matrices :

$$C_{m1} = \begin{pmatrix} 1 & 0 & 0 \\ 0 & 1 & 0 \end{pmatrix} \tag{14}$$

$$C_{m2} = \begin{pmatrix} 0 & 1 & 0 \\ 0 & 0 & 1 \end{pmatrix} \tag{15}$$

$$C_{m3} = \begin{pmatrix} -\sin\Phi & \cos\Phi & 0 \\ \cos\Phi\cos\Theta & \sin\Phi\cos\Theta & \sin\Theta \end{pmatrix} \tag{16}$$

Equivalently, the assumed projection geometry may be represented by $\tilde{C}_m$, obtained by stacking the matrix representations of the linear operators C_{mi} as discussed in Section 2.1. Thus, this assumed geometry provides us with a reasonable choice for the matrix $\tilde{C}_m$ which can be used in our reconstructions.

Two-Dimensional Processing

Our alternative method of combining the three views of data to estimate the ejection fraction is to process each view individually as a two-dimensional problem. That is, we use a model identifier to individually estimate the dynamics of the ellipses observed in each view. The outcome of the model identifier is then used to provide a dynamic model for the smoothing-filter-based reconstruction of the ellipse trajectory in that view. Based on the smoothed ellipses, the apparent two-dimensional "ejection fraction" for each view is calculated. Note for such two-dimensional processing, the goal is to *estimate* two-dimensional ellipsoids from noisy observations of the ellipsoids themselves, in contrast to the three-dimensional case where the projections were used as the observations in directly *reconstructing* the three-dimensional ellipsoid. Thus, for

two-dimensional processing, the matrix $\tilde{C}$ in (8) which relates the ellipsoid to the measurements, is given by the identity. The two-dimensional ejection fraction obtained from each view measures only the contraction of the ellipsoid in the plane of the projection and neglects all contraction perpendicular to the plane of the projection. Thus, each two-dimensional ejection fraction actually underestimates the underlying three-dimensional ejection fraction. From the two-dimensional ejection fractions of each view, it is possible to approximate the three-dimensional ejection fraction using the formula given in (9), which implicitly assumes that the true projection geometry corresponds to projections onto three orthogonal planes.

3 SIMULATIONS

In this section, we present simulation results which illustrate the methods outlined in Section 2. First, simulated data are used to evaluate the performance of the model identification scheme. Next, simulations are used to investigate the effect of the dynamic model mismatch introduced by the coarse approximation provided by the model identifier and investigate methods to minimize the error introduced by this dynamic model mismatch. Finally, an angle sensitivity analysis is presented to show that the assumed projection geometries should introduce a minimal error into the ejection fraction estimates.

3.1 Model Identification

Let us turn now to the evaluation of the model identification scheme as a method to determine which of several models is the best approximation to the true ellipsoid dynamics. For this evaluation, the model identifier will be based on two hypothesized models only. Two experiments were conducted. Experiment #1 is designed to investigate the performance of the

model identifier when one of the hypothesized models exactly matches the true dynamics and the separation between the two models is varied. Experiment #2 is designed to characterize the performance of the model identifier when the true ellipsoid dynamics varies between the two hypothesized models.

For both Experiment #1 and #2 the following simulation setup is assumed. A computer simulated, three-dimensional ellipsoid and its projection measurements are generated as described by (7) and (8). The initial ellipsoid has semi-axis lengths of 8, 7.2, and 8; these ellipsoid axes are aligned with the x-, y-, z-axes, respectively. The true dynamics are expressed by matrices $A_t(k)$ which are of the form given in (17) :

$$A_t(k) = \begin{cases} c_t\, \mathcal{R}(\theta_t) & \text{for } 1 \leq k \bmod 16 + 1 \leq 8 \\ 1/c_t\, \mathcal{R}(-\theta_t) & \text{for } 9 \leq k \bmod 16 + 1 \leq 16 \end{cases} \tag{17}$$

Here $\mathcal{R}(\cdot)$ describes rotation about the x-axis and is a generalization of the last term in (5); c_t and θ_t are the true rates of contraction and rotation, respectively. These true dynamics generate a shrinking/rotating and expanding/rotating ellipsoid. Since the myocardial perfusion data consists of 16 frames per cycle, the simulated ellipsoid cycle was chosen to be 16. The ejection fraction that corresponds to the true model (17) will be denoted EF_t. The measurements, as described by (3), are taken to be noisy projections onto three orthogonal planes which are aligned with the ellipsoid axes. This projection geometry corresponds to projections on the xy-, yz-, and xz-planes, respectively and is captured by the matrices C_1, C_2, C_3 which are given as in (14)-(16) with $\Phi = \Theta = 0$. Equivalently, these linear operators may be represented by the matrix $\tilde{C}$, which is obtained by stacking the matrix representations of C_1, C_2 and C_3 as described in Section 2.1. The model identifier is initialized with the linear least squares estimate of the ellipse at time $k = 0$ based on data at $k = 0$. We would like to set the initial

error covariance, P_0, to be high to indicate that our confidence in this initial estimate is low. Therefore, our initialization is given by :

$$\hat{x}(1|0) = (\tilde{C}^T\tilde{C})^{-1}\tilde{C}^T y(1) \tag{18}$$

$$P_0 = 5R \tag{19}$$

where $R = rI$ is the measurement noise variance.

The model identifier is based on two hypothesized dynamical models with associated dynamic matrices A_1 and A_2. These hypothesized dynamics have corresponding contraction rates of c_1 and c_2 and rotation rates of θ_1 and θ_2, respectively. The matrices A_1 and A_2 are of the same form as (17) with true contraction and rotation rates replaced by the corresponding modeled contraction and rotation rates. The ejection fractions corresponding to the two hypothesized models, A_1 and A_2, will be denoted as EF_1 and EF_2. Experiments #1 and #2 differ in which of the values c_t, c_1, c_2, θ_t, θ_1, and θ_2 are held fixed and which are varied.

Both sets of experiments will be carried out for several levels of measurement noise variance. This noise variance will be held constant throughout the experiment interval. We will categorize each noise level by the initial signal-to-noise ratio (ISNR) defined as :

$$\mathrm{ISNR} = \sqrt{\frac{\|x(1)\|^2}{n(n+1)r/2}} \tag{20}$$

where $x(1)$ is the vector representation of the ellipsoid at time $k = 1$, n is the dimension of x, and r is the variance of the measurement noise. The initial signal-to-noise ratios (ISNR) for each of the four measurement noise levels under consideration are listed in Table 1. These measurement noise levels range from almost no noise at ISNR #1 to a level of noise comparable in magnitude to that of the ellipsoid itself at ISNR #4 (i.e. so that the values of the noise are on the same order as the values in $x(1)$ itself). The noise levels are chosen to cover the range of the noise expected from a typical ellipse extraction routine.

ISNR #1	22.36
ISNR #2	12.57
ISNR #3	7.07
ISNR #4	3.98

Table 1: Initial signal-to-noise ratio for several measurement noise levels.

Experiment #1

The objective of Experiment set #1 is to investigate how sensitive the model identifier is to the separation of the hypothesized ejection fractions when one of the hypothesized dynamic models exactly matches the dynamics used to create the set of ellipses. Even though such a scenario does not exist in the real world, this exercise is useful since it illustrates the sensitivity performance of the model identification scheme. In Experiment set #1, the true dynamics and ejection fraction always equals that associated with hypothesized Model #1 (i.e. $c_t = c_1$, $\mathrm{EF}_t = \mathrm{EF}_1$) and c_2 is allowed to vary. For Experiment set #1, neither the true nor modeled dynamics include rotation (i.e. $\theta_t = \theta_1 = \theta_2 = 0$). The hypothesized models have associated ejection fractions that yield an EF separation which is given by $\mathrm{EF}_s = \mathrm{EF}_1 - \mathrm{EF}_2 = \mathrm{EF}_t - \mathrm{EF}_2$. The performance of the model identifier is evaluated at the four signal-to-noise levels of Table 1 as this separation between the two hypothesized models is decreased. To control the complexity of this experiment, the projection geometry was assumed known to the model identifier. Figure 3 shows the number of realizations out of 100 that correctly identify Model #1 as a function of the separation between the two hypothesized ejection fractions and the measurement noise level. These results indicate that for high signal-to-noise ratio the model identifier always chooses the correct model regardless of the separation between the two hypothesized ejection fractions. For lower signal-to-noise ratios (i.e. ISNR #2, ISNR #3, ISNR #4), the performance of the model identifier deteriorates as the separation of the two models decreases. For this specialized

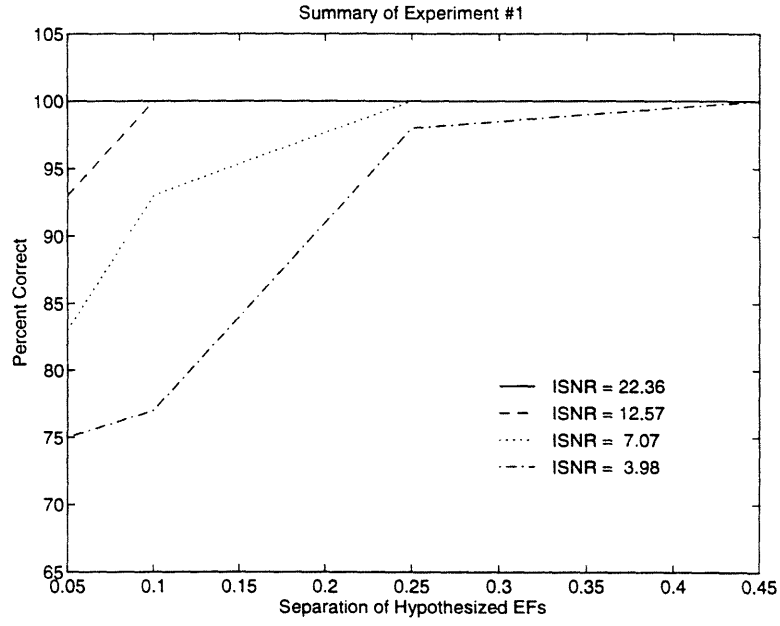

Figure 3: Model identification experiment #1 results.

case, these results indicate that 75% correct identification can be obtained over an extremely wide range of separations even for low signal-to-noise ratio.

Experiment #2

The objective of Experiment set #2 is to evaluate the performance of the model identification scheme when the true ellipsoid dynamics include contraction, expansion and rotation, but the hypothesized models are simpler, including only contraction and expansion at a rate that differs from the true contraction/expansion. To study this case, the dynamics and thus, ejection fractions of the two hypothesized models are fixed and the true dynamics vary so that the true ejection fraction varies between those of the two hypothesized models. Again, this study includes an investigation of the effect of measurement noise on the model identification approach. The two hypothesized dynamic models are captured by dynamic matrices A_1 and A_2 which are of the form (17) with hypothesized contraction rates of $c_1 = .9572$ and $c_2 = 0.9907$ which correspond to ejection fractions of EF_1=0.65 and EF_2=0.20. These modeled dynamics

do not include rotation (i.e. $\theta_1 = \theta_2 = 0$). The true ellipsoid dynamics are also of the form given in (17) with values of c_t in the range from 0.9605 to 0.9892, which correspond to values of EF_t from 0.62 down to 0.23. The true dynamics include a rotation at each step of $\theta_t = \pi/54$ about the x-axis, which implies a total rotation over the eight time steps of approximately $\pi/6$. This experiment was repeated 100 times for each value of c_t. Figure 4 shows the percent of realizations that picked model #1 given all the data for each value of ejection fraction of the true ellipsoid dynamics. For the high signal-to-nose ratio case (ISNR #1), the model identifier performs as follows: if $\mathrm{EF}_t \gtrsim 0.47$, then model #1 is chosen; if $\mathrm{EF}_t \lesssim 0.4$, then model #2 is chosen; if $0.4 \lesssim \mathrm{EF}_t \lesssim 0.47$, then the outcome is uncertain. For lower signal-to-noise ratios, (ISNR #2, ISNR #3, ISNR #4), the results indicate that the performance of the model identifier deteriorates and the transition region widens. However, outside of these relatively narrow transition regions, the model identifier performs as expected, by choosing the hypothesized model which more closely approximates the true ellipsoid dynamics and, in particular, more closely matches the true ejection fraction. These results show that even though the true ellipsoid dynamics, which include contraction, expansion and rotation, are more complicated than the hypothesized dynamics, which only include contraction and expansion, the model identifier still picks the model whose dynamics more closely matches the true ellipsoid dynamics. Thus, the model identifier based on simple hypothesized models will adequately capture dynamics reflecting our quantity of interest, i.e. the ejection fraction.

3.2 Dynamic Model Mismatch

Next, we investigate the effects of dynamic model mismatch. The objectives of this study are to evaluate the error introduced by dynamic model mismatch and to investigate methods to minimize the error. As in the evaluation of the model identifier, a computer simulated

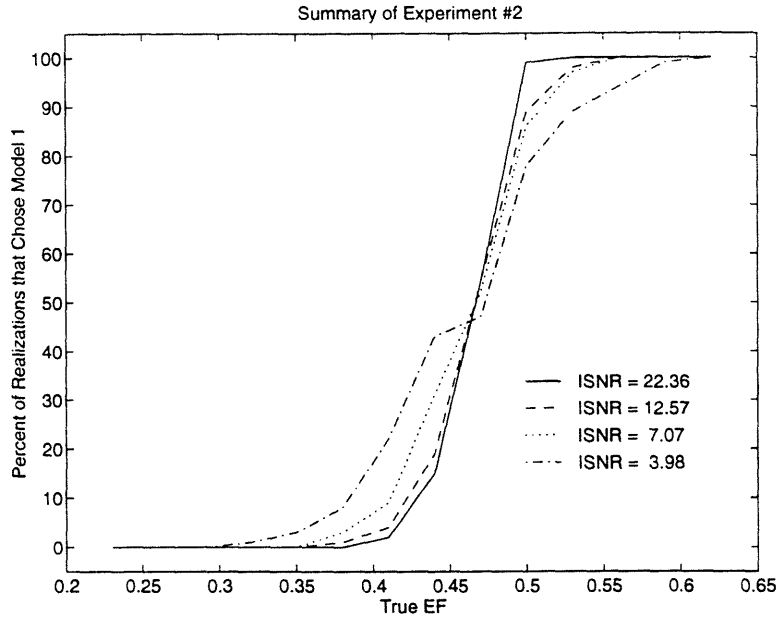

Figure 4: Model identification experiment #2 results.

three-dimensional ellipsoid and its noisy measurements are generated as described in (7), (8), and Table 1. The initial ellipsoid, true projection geometry, smoothing filter initialization are exactly as described in Section 3.1. The true dynamics include periodic contraction for the first half cycle and expansion for the second half cycle without rotation. Specifically, these dynamics are of the form (17) with $c_t = .9615$ and $\theta_t = 0$. The true dynamics yield an ejection fraction $\mathrm{EF}_t = 0.60$. A smoothing filter based on the Rauch-Tung-Striebel smoothing algorithm is implemented to reconstruct the three-dimensional ellipsoid from the noisy two-dimensional projections. This smoothing filter is based on the periodic dynamic model given by matrices $A_m(k)$ of the form (17) with modeled contraction and rotation rates c_m and θ_m. In reality, a method such as model identification might have been used to choose these matrices $A_m(k)$. For the experiment, these model dynamics consist of simple periodic contraction for the first half cycle and expansion for the second half cycle chosen to yield a corresponding intrinsic ejection fraction of $\mathrm{EF}_m = 0.70$, which corresponds to $c_m = .9515$. The modeled dynamics

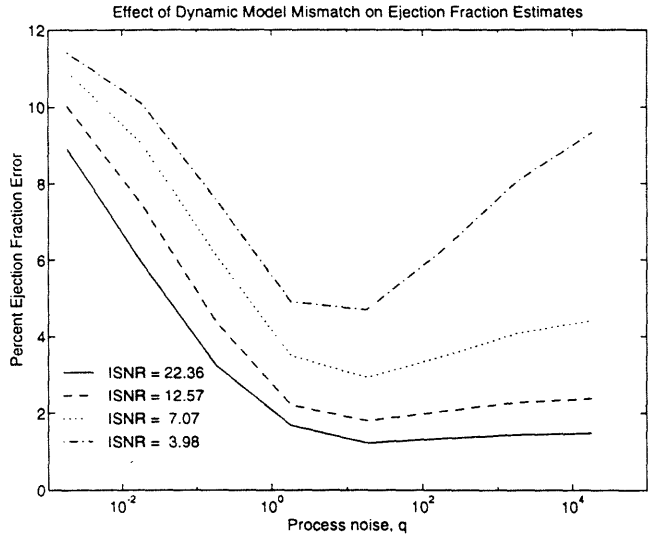

Figure 5: Ejection fraction error using an assumed dynamic model.

include no rotation ($\theta_m = 0$).

The ellipsoids are reconstructed from noisy measurements using a Rauch-Tung-Striebel smoothing filter based on the dynamic model described by A_m. From the reconstructed ellipsoids, an estimated ejection fraction value is calculated. As discussed in Section 2.2, it is possible to "tune" the filter by adjusting the value of q, the process noise variance. The results of this simulation are given in Figure 5, which shows the variation of the percent error in the ejection fraction estimate with q. This percent ejection fraction error is defined as

$$\text{Percent EF Error} = \frac{|\text{True EF} - \text{Estimated EF}|}{\text{True EF}} \tag{21}$$

Note that the percent ejection fraction error is flat for a wide range of q even at high levels of measurement noise. In particular, at the highest noise level it is possible to reduce the percent ejection fraction error by a factor of two by appropriate choice of q. These results illustrate that q may be effectively used to minimize the error introduced by dynamic model mismatch. That is, q may be used to vary the amount of smoothing introduced by the filter, though we do not in fact bother to do this in our use of real data to follow.

3.3 Projection Geometry–A Sensitivity Analysis

Finally, we investigate the sensitivity of the three-dimensional and two-dimensional data processing approaches (described in Section 2.2) as the true projection geometry is varied. Each of these data processing approaches is based on an assumed projection geometry, also described in Section 2.2. In this section, we investigate the error in the ejection fraction estimate introduced by the assumed projection geometries underlying both the three-dimensional and two-dimensional processing of the projection data, over a wide range of true projection geometries.

The experimental procedure used for this sensitivity analysis is as follows. We generate computer simulated, dynamically evolving ellipsoids. Observations of these ellipsoids are taken as noise-less projections at a range of true projection geometries. For each of these true projection geometries, the observations are processed using both the three-dimensional and two-dimensional methods. The ejection fraction estimate is formulated for both methods and compared to the true ejection fraction. Note that noise-less observations and static reconstruction are used so that the uncertainty introduced by imperfectly known dynamics is eliminated.

The computer simulated, dynamically evolving ellipsoid has the following characteristics. The parameters for this ellipsoid are chosen so that our experiment is a *worst case* sensitivity analysis in the *physiological* sense. That is, a real left ventricle is expected to be much less eccentric than the ellipsoids being considered here; and real left-ventricular dynamics are expected to display only a slight rotation instead of the gross rotation used here. Denote the fully expanded and fully contracted simulated ellipsoids by their vector representations $x(k_{\max})$ and $x(k_{\min})$, respectively. The semi-axis lengths and long axis orientations of $x(k_{\max})$ and $x(k_{\min})$

	Semi-Axis Lengths	Long Axis Orientation
$x(k_{\max})$	10, 7, 7	(-0.5,-0.5, 0.7071)
$x(k_{\min})$	7.37, 5.16, 5.16	(-0.5,0.5, 0.7071)

Table 2: Axis lengths and orientations for $x(k_{\max})$ and $x(k_{\min})$.

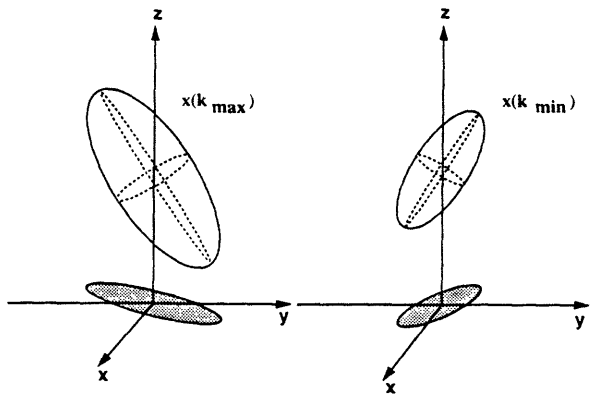

Figure 6: The ellipsoids used for the angle sensitivity analysis. The shadows are shown to emphasize the orientation of the ellipsoid.

are given in Table 2. Thus, the dynamics that relate $x(k_{\max})$ and $x(k_{\min})$ consist of an isotropic scaling by 0.7368 and a rotation of 90° about the z-axis. These dynamics yield an ejection fraction of 0.60. Both $x(k_{\max})$ and $x(k_{\min})$ are shown in Figure 6.

For this sensitivity analysis, we consider the following range of true projection geometries, which are used to generate the data (the projections of the ellipsoid). These true projection geometries consist of three projection planes. The first two are given by the (orthogonal) xz- and yz-planes and the third plane is specified by (13) with $\Phi = 45°$ and $0° < \Theta < 90°$. Note that each of these true projection geometries may be represented by a set of matrices of the same form as (14) - (16) with $\Phi = 45°$ and $0° < \Theta < 90°$ as described above which we denote as $\{C_{t1}, C_{t2}, C_{t3}\}$. This situation captures our prior belief that in a real acquisition two of the projections are relatively fixed and orthogonal (the LAT and ANT projections) while the third (LAO) contains the greatest amount of variability. For each of these true projection

geometries, we evaluate the percent ejection fraction error introduced by both the two- and three-dimensional processing approaches.

For the three-dimensional processing approach, the three views are processed together as a single reconstruction problem. Recall that the observations of the ellipsoids are noise-less projections onto the planes that define the true projection geometry. For this reconstruction, we assume a projection geometry which consists of three projection planes as described in Section 2.2. Recall that this assumed projection geometry is described by the set of matrices $\{C_{m1}, C_{m2}, C_{m3}\}$ (as in (14) - (16) with $\Phi = \Theta = 45°$) or equivalently $\tilde{C}_m$ (as described in Section 2.1). Because the observations are noise-less, a static reconstruction method is used which gives $\hat{x}(k) = (\tilde{C}_m^T \tilde{C}_m)^{-1} \tilde{C}_m^T y(k)$ where $y(k)$ are the observations of the ellipsoid. From the reconstructed ellipsoids $\hat{x}(k_1)$ and $\hat{x}(k_2)$, the estimated ejection fraction is calculated using (1).

For the two-dimensional processing approach, each view is processed individually. That is, the areas of the projections of $x(k_{\max})$ and $x(k_{\min})$ in each view are used to calculate the two-dimensional ejection fraction of that view. Again, because the projections are noiseless, we do not need to smooth the data. Then, the three, two-dimensional ejection fractions are combined using (9) to obtain a three-dimensional ejection fraction estimate.

The results from this angle sensitivity analysis are presented in Figure 7. For the three-dimensional processing, the results show that for a wide range of true projection geometries the error in the ejection fraction estimate is small, less than 10%. While not as impressive as the three-dimensional results, the two-dimensional results show that the ejection fraction errors are less than 12% for a wide range of true projection geometries. Recall, however, that this sensitivity analysis is a worst case study. In general, the two-dimensional processing will be less affected by variations than is indicated in Figure 7.

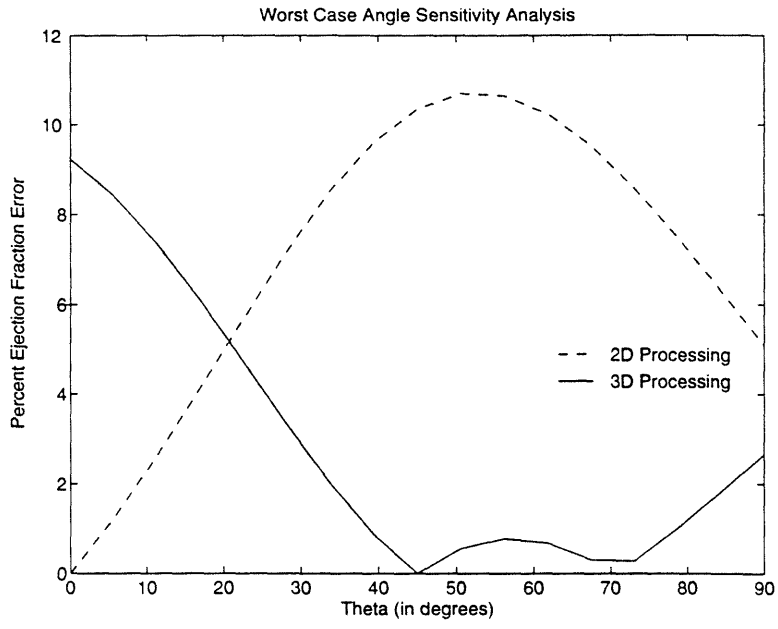

Figure 7: Worst case angle sensitivity analysis results.

4 APPLICATION TO REAL DATA

In the previous sections, the proposed methods to overcome imprecisely known dynamics and projection geometry were outlined and tested on simulated data. In this section, the same methods will be applied to ellipses extracted from real myocardial perfusion data to calculate the ejection fraction of the left ventricle for 14 individuals.

Note once again that these approaches require as their inputs ellipses that have been extracted from the myocardial perfusion images via a preprocessing step. Since the focus of this work is the estimation of dynamically evolving ellipsoids, we assume that such an ellipse extraction phase which also provides statistical characterization of the measurement noise (i.e. R, the variance of the measurement noise) is available. For this work, a very simple ellipse extraction routine is used (see [20] for details) and the measurement noise variance is assumed to be $R = rI$ where r is chosen empirically. Further, even for this simple ellipse extraction method, the results are promising.

In addition, the outputs of the model identifier and smoothing filter are affected by the variance of the process noise, Q, assumed to be qI. It would also be logical to use a value of q that is in the range that minimizes the effect of residual dynamic model mismatch for the given r, as was illustrated in Section 3. Again, since we do not have an estimate of r, we have used a value of q that was chosen empirically [3]. Specific values for the parameters r, q used for each case are given in the respective section discussing that case.

Recall that there exist many techniques to estimate ejection fraction using other imaging techniques. In this section, the ejection fraction calculated from myocardial perfusion images using our methods is compared to a "gold standard" (GS) ejection fraction obtained using a technique known as multiple-gated blood pool (or MUGA). Thus, the ejection fraction estimate based on myocardial perfusion images is evaluated by calculating the sample correlation[4], $\rho_s(x, y)$, with the GS value.

4.1 Two-Dimensional Processing

In two-dimensional processing of the data, each view is processed individually. That is, a model identification scheme is applied to each view to determine which of three hypothesized models best approximates the true ellipse dynamics. Next, the model chosen by a simple vote of the outputs of the model identifier for the three views is used in a Rauch-Tung-Striebel smoothing filter to reconstruct the underlying ellipses. From the reconstructed ellipses, an effective two-dimensional ejection fraction for each view is found. Then, using the formula given in (9), an estimate of the three-dimensional ejection fraction is calculated.

[3] An alternative to these empirically chosen values for the parameters r, q, which control smoothing, is discussed in [21].

[4] Here sample correlation coefficient is given as $\rho_s(x, y) = \frac{\mathrm{cov}_s(x,y)}{\sigma_{s,x}\sigma_{s,y}}$ where $\mathrm{cov}_s(x, y)$ refers to the sample covariance of x and y and $\sigma_{s,x}$ and $\sigma_{s,y}$ are the sample standard deviations of x and y, respectively [22].

The model identification scheme is implemented in the following way. For each of the three views, the input to the model identifier consists of the set of 16 ellipses extracted from the raw data for that view. The observations are of the ellipses themselves; therefore, the matrix C that specifies the projection geometry in (8) given by the identity. Three hypothesized models are used which yield hypothesized ejection fractions EF_1=0.60, EF_2= 0.40 and EF_3= 0.20, respectively. The specific dynamics used for each of these hypothesized models are of the form of (17), where the parameters c_m are chosen so that the time (i.e. frame) of maximal contraction matches the the corresponding time determined by eye from the data (i.e. so end systole of the model matches end systole of the heart data). Once again, the model identifier is initialized as in (18) and (19). The measurement noise variance r is chosen empirically to be 100. The value of q is set to zero to accentuate the difference between the three models. The dynamic model used for the smoothing phase is then chosen by a simple vote of the individual decisions of the model identifier for the three views.

Next, the Rauch-Tung-Striebel smoothing filter for each view is implemented based on the dynamic model chosen by the model identifier phase. For the smoothing filter, the empirically chosen values of r/q is 2. Again, the initialization of the smoothing filter is as given in (18) and (19). The three-dimensional ejection fraction estimate for each individual is obtained from the effective two-dimensional ejection fraction estimates using (9). Each two-dimensional ejection fraction is obtained using (1) (with volumes replaced by areas).

Figure 8 compares the two-dimensional based estimated ejection fraction values to the GS ejection fraction values for each of 14 patients. The two-dimensional based ejection fraction estimates are quite good. In Figure 8, the solid line is the best fit line to the 14 data points and the dashed line is the unit slope line. For the sample size of 14 and the data presented in Figure 8, the sample correlation coefficient is calculated to be ρ_s=0.9135. In addition, the

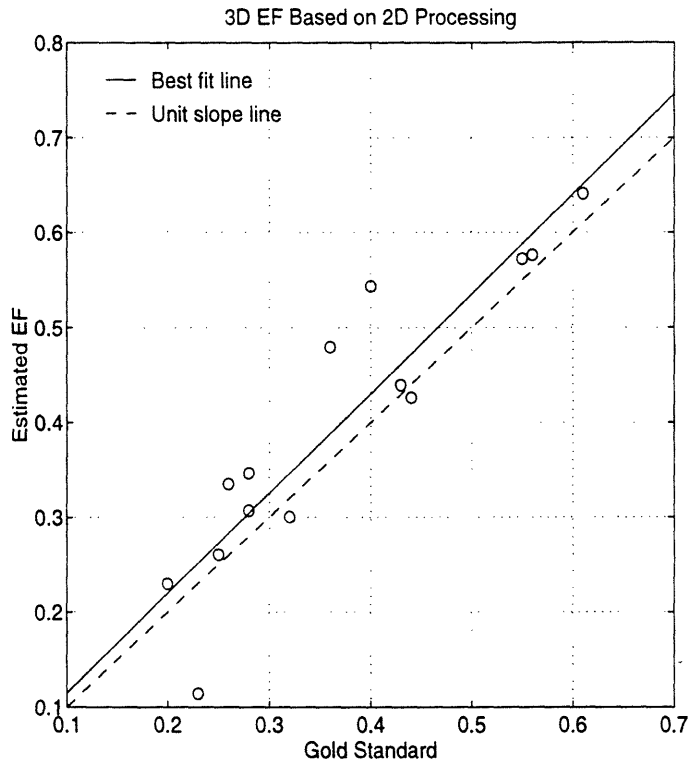

Figure 8: Comparison of GS and 2D-based estimated ejection fraction for 14 patients.

95% confidence region [23] is given as $0.7431 < \rho < 0.9727$.

4.2 Three-Dimensional Processing

In this section, model identification and smoothing-filter reconstruction are applied to directly combine the set of two-dimensional observations as projections of a single three-dimensional ellipsoid that approximates the left ventricle. Based on the reconstructed dynamically evolving, three-dimensional ellipsoid that approximates the left ventricle, an estimate of the ejection fraction is calculated. For this processing, an assumed projection geometry is used in which ANT and LAT views correspond to projections onto orthogonal planes and the LAO view corresponds to a projection onto a plane that is tilted by $\pi/4$ from the plane that is orthogonal to both the ANT and LAT planes, as discussed in Section 2.2 and shown in Figure 2. The

normal to this modelled LAO plane is given as in (13) with $\Theta = \Phi = 45°$.

The model identifier processes the combined data set from all three views for each individual to determine which of the hypothesized models should be used to model the true dynamics in the smoothing-filter-based reconstruction stage. The hypothesized models and filter initializations are analogous to those described in Section 4.1. The values of r and q are chosen to be 100 and zero, respectively. The Rauch-Tung-Striebel smoothing filter, which is implemented based on the dynamic model chosen by the model identifier, uses $r/q = 2$. The three-dimensional ejection fraction estimate for each individual is then obtained from the change volume of these ellipsoids using (1).

Figure 9 compares the GS ejection fraction values and the ejection fraction estimates based on the three-dimensional dynamic approach. For the sample size of 14 and the data presented in Figure 9. Again, this processing provides reasonable ejection fraction estimates. The sample correlation coefficient is calculated to be ρ_s=0.8527 with a 95% confidence interval of 0.5883< ρ <0.9524. These results indicate that the three-dimensional processing did not perform as well as the two-dimensional processing, which seems counter-intuitive. One explanation is that in the three-dimensional processing the interaction between the imperfectly known dynamics and the imperfectly known projection geometry may result in this greater error. In contrast, for the two-dimensional processing, the dynamics and projection geometry are handled independently. Further study with a larger sample size will be needed to fully understand this phenomenon.

5 CONCLUSIONS

This paper has outlined a model-based, statistical approach to obtain a dynamic estimate of left-ventricular ejection fraction from a gated set of planar myocardial perfusion images. This

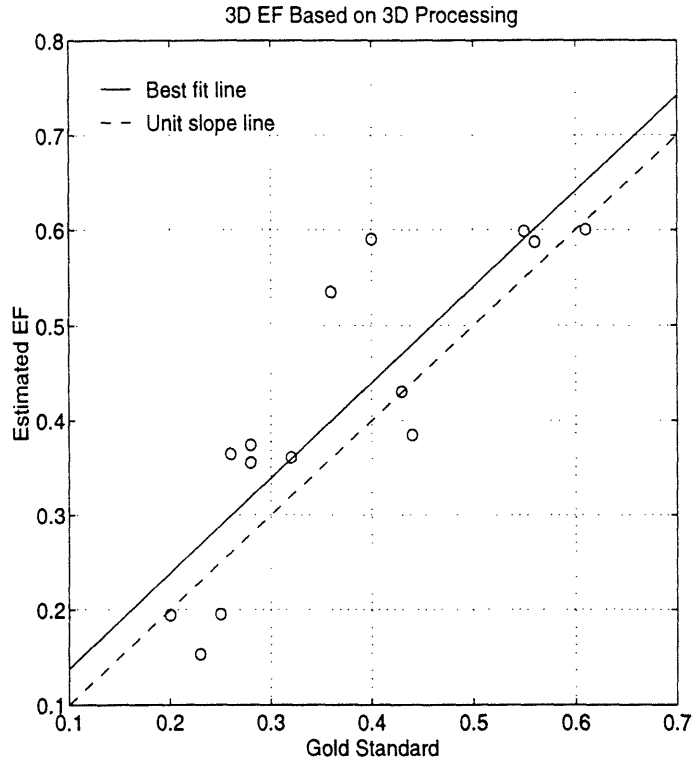

Figure 9: Comparison of GS and 3D-based estimated ejection fraction for 14 patients.

method was proposed as a safer, more cost-effective, and more robust alternative to currently used techniques. Because the modeling assumptions are explicitly stated and quantitatively used, it is possible to investigate the sensitivity of the ejection fraction error with respect to these assumptions. Simulations were used to demonstrate that the error due to imperfectly known dynamics and projection geometry could be minimized by appropriate choices of the smoothing filter parameters. In addition, these methods were shown to give accurate estimates of ejection fraction for levels of measurement noise that are comparable to those expected in real data.

These methods were then used to estimate ejection fraction from real myocardial perfusion images. Although a relatively small sample size was used, the smoothing-filter-based ejection fraction estimates showed a high degree of correlation with the GS ejection fraction estimates.

Finally, note that while our goal here is the calculation of ejection fraction, one can imagine directly using the dynamic shape estimates provided by our methods for diagnostic purposes.

Future work may include the following further studies and improvements to the methods described in this paper. A larger sample size would be useful in obtaining tighter confidence bounds on the estimated correlation coefficient. As previously mentioned, our dynamically-based smoothing techniques may be directly applied to other imaging modalities to obtain ejection fraction estimates. Further studies might evaluate these methods as applied to images obtained from other modalities such as MUGA. In addition, more hypothesized models may be included in the model identification phase so that the assumed ejection fraction used in the smoothing-filter-based reconstruction is closer to the true ejection fraction. Another investigation might consider the use of a model identification approach (similar to the one we used to determine the ellipsoid dynamics) to determine the projection geometry. Finally, a circular smoothing algorithm might be considered which incorporates the additional constraint that the ellipsoid estimate at initial and final points of the cardiac cycle should be the same; thus, capturing a true periodicity assumption on the cardiac dynamics.

ACKNOWLEDGMENTS

The authors would like to thank Charles Boucher, M.D., and David Chesler, Sc.D., who provided the myocardial perfusion images used in this work.

References

[1] Y. Bresler, J. A. Fessler, and A. Macovski, "Model-based estimation techniques for 3-D reconstruction from projections," *Machine Vision and Applications*, vol. 1, pp. 115–126,

1988.

[2] Y. Bresler and A. Macovski, "Three-dimensional reconstruction from projections with incomplete and noisy data by object estimation," *IEEE Transactions on Acoustics, Speech, and Signal Processing*, vol. ASSP-35, 1987.

[3] W. C. Karl, G. C. Verghese, and A. S. Willsky, "Reconstructing ellipsoids from projections." Submitted to CGVIP-Graphical Models and Image Processing.

[4] J. L. Prince, *Geometric Model-Based Estimation from Projections.* PhD thesis, Massachusetts Institue of Technology, January, 1988.

[5] D. J. Rossi and A. S. Willsky, "Reconstruction from projections based on detection and estimation of objects-parts I and II: Performance analysis and robustness analysis," *IEEE Transactions on Acoustic, Speech, and Signal Processing*, vol. ASSP-32, no. 4, pp. 886–906, 1984.

[6] C. A. Boucher, "Detection and location of myocardial infarction using technetium-99m sestamibi imagin at rest," *American Journal of Cardiology*, vol. 66, pp. 32E–35E, October 1990.

[7] J. Heo, G. Hermann, A. Iskandrian, A. Askenase, and B. Segal, "New myocardial perfusion imaging agents: Description and applications," *American Heart Journal*, pp. 1111–1117, May 1988.

[8] A. Sinusas, G. Beller, W. Smith, E. Vinson, V. Brookeman, and D. Watson, "Quantitative planar imaging with technetium-99m methoxyisobutyl isonitrile: Comparison of uptake patterns with thallim-201," *The Journal of Nuclear Medicine*, pp. 1456–1463, 1989.

[9] S. R. Underwood, S. Walton, P. J. Laming, P. H. Jarrit, P. J. Ell, R. W. Emanuel, and R. H. Swanton, "Left ventricular volume and ejection fraction determined by gated blood pool emission tomography," *British Heart Journal*, vol. 53, pp. 216–222, 1985.

[10] R. H. Eich, *Introduction to Cardiology.* Harper & Row, 1980.

[11] I. Mirsky, D. Ghista, and H. Sandler, *Cardiac Mechanics: Physiological, Clinical, and Mathematical Considerations.* John Wiley & Sons Inc., 1974.

[12] E. Goldberger, *Essentials of Clinical Cardiology.* J.B. Lippincott Co., 1990.

[13] A. Gelb, ed., *Applied Optimal Estimation.* The MIT Press, 1988.

[14] A. and E. Delp, "Digital two-dimensional echocardiography," in *Digital Cardiac Imaging*, ch. 11, Martinus Nijhoff Publishers, 1985.

[15] A. Aisen and A. Buda, "Magnetic resonance imaging of the heart," in *Digital Cardiac Imaging* (A. Buda and E. Delp, eds.), ch. 15, Martinus Nijhoff Publishers, 1985.

[16] M. H. Davis, B. Rezaie, and F. L. Weiland, "Assesment of left ventricular ejection fraction from Technitium-99m-methoxy isobutyl isonitrile multiple-gated radionuclide angiocardiography," *IEEE Transactions on Medical Imaging*, vol. 12, pp. 189–199, June 1993.

[17] R. Chan and W.-C. Siu, "Fast dectection of ellipses using chord bisectors," in *IEEE International Conference on Accoustics, Speech, and Signal Processing*, pp. 2201–2204, 1990.

[18] J. Porrill, "Fitting ellipses and predicted confidence envelopes using a bias corrected Kalman filter," *Image and Vision Computing*, vol. 8, pp. 37–41, February 1990.

[19] H. K. Yuen, J. Illingworth, and J. Kittler, "Detecting partially occluded ellipses using the Hough transform," *Image and Vision Computing*, vol. 7, pp. 31–37, February 1989.

[20] S. Jaggi, "Estimation of dynamically evolving ellipsoids with applications to cardiac imaging," Master's thesis, Massachusetts Institue of Technology, September, 1992.

[21] J. A. Fessler, "Nonparametric fixed-interval smoothing with vector splines," *IEEE Transactions on Signal Processing*, vol. 39, pp. 852–859, April 1991.

[22] R. Anderson and T. Bancroft, *Statistical Theory in Research.* McGraw-Hill Inc., 1952.

[23] H. D. Brunk, *An Introduction to Mathematical Statistics.* Xerox College Publishing, 1975.

[24] J. Juni and A. Buda, "Radionuclide imaging of the heart," in *Digitial Cardiac Imaging* (A. Buda and E. Delp, eds.), ch. 13, Martinus Nijhoff Publishers, 1985.

[25] L. Opie, *The Heart.* Grune & Stratton, Inc., 1984.

[26] G. Strang, *Linear Algebra and Its Applications.* Harcourt Brace Jovanovich, 1988.

[27] E. Jacobs, *Medical Imaging : A Concise Textbook.* Igaku-Shoin, 1987.

[28] I. Meschan and D. Ott, *Introduction to Diagnostic Imaging.* W.B. Saunders Company, 1984.

List of Figures